BIOCHEMISTRY

 Volume 47, Number 9 March 4, 2008

Articles

Nucleotide Selectivity Opposite a Benzo[*a*]pyrene-Derived N^2-dG Adduct in a Y-Family DNA Polymerase: A 5′-Slippage Mechanism†

Pingna Xu,‡ Lida Oum,§ Nicholas E. Geacintov,§ and Suse Broyde*,‡

Department of Biology, New York University, 1009 Silver Center, 100 Washington Square East, New York City, New York 10003, and Department of Chemistry, New York University, 1001 Silver Center, 100 Washington Square East, New York City, New York 10003

Received September 9, 2007

ABSTRACT: The Y-family DNA polymerase Dpo4, from the archaeon bacterium *Sulfolobus solfataricus*, is a member of the DinB family, which also contains human Pol κ. It has a spacious active site that can accommodate two templating bases simultaneously, with one of them skipped by the incoming dNTP. Assays of single dNTP insertion opposite a benzo[*a*]pyrene-derived N^2-dG adduct, 10*S*(+)-*trans-anti*-[BP]-N^2-dG ([BP]G*), reveal that an incoming dATP is significantly preferred over the other three dNTPs in the TG_1*G_2 sequence context. Molecular modeling and dynamics simulations were carried out to interpret this experimental observation on a molecular level. Modeling studies suggest that the significant preference for dATP insertion observed experimentally can result from two possible dATP incorporation modes. The dATP can be inserted opposite the T on the 5′ side of the adduct G_1*, using an unusual 5′-slippage pattern, in which the unadducted G_2, rather than G_1*, is skipped, to produce a −1 deletion. In addition, the dATP can be misincorporated opposite the adduct. The 5′-slippage pattern may be generally facilitated in cases where the base 3′ to the lesion is the same as the adducted base.

Bulky carcinogen−DNA adducts are well-known to impede replication by traditional high-fidelity replicative DNA polymerases, whereas Y-family DNA polymerases play a key role in bypassing such DNA lesions (*1*–*7*). DNA polymerase IV (Dpo4)[1] is a Y-family bypass polymerase from the archaeon bacterium *Sulfolobus solfataricus* and belongs to the DinB family, of which human Pol κ is a member (*8, 9*). The structure of Dpo4 has been extensively studied by X-ray crystallography methods, and a number of crystal structures in the form of binary enzyme−primer/template DNA complexes and ternary enzyme−primer/template DNA−dNTP complexes, with and without DNA lesions, have been solved (*10*–*20*). These studies have revealed a spacious and solvent-accessible active site that is significantly different from that of replicative polymerases; in the latter, the correct dNTP binding is achieved by an induced-fit mechanism, with the enzyme in the ternary complex tightly wrapped around the nascent base pair to essentially exclude the solvent (*21*–*24*). The crystal structures

† This work was supported by National Institutes of Health (NIH) Grant 5RO1 CA 28038 (to S.B.) and 2RO1 CA 099194 (to N.E.G).

* To whom correspondence should be addressed. Telephone: (212) 998-8231. Fax: (212) 995-4015. E-mail: broyde@nyu.edu.

‡ Department of Biology.

§ Department of Chemistry.

[1] Abbreviations: PAH, polycyclic aromatic hydrocarbon; BP, benzo[*a*]pyrene; BPDE, 7,8-dihydroxy-9,10-epoxybenzo[*a*]pyrene diol epoxide; (+)-*anti*-BPDE, (+)-7(*R*),8(*S*),9(*S*),10(*R*)BPDE; [BP]G*, (+)-*trans-anti*-[BP]-N^2-deoxyguanosine; dNTP, 2′-deoxynucleotide triphosphate; Dpo4, *Sulfolobus solfataricus* DNA polymerase IV; CG, conjugate gradient; SD, steepest descent; MD, molecular dynamics; rmsd, root-mean-square deviation.

10.1021/bi701839q CCC: $40.75
Published on Web 02/09/2008

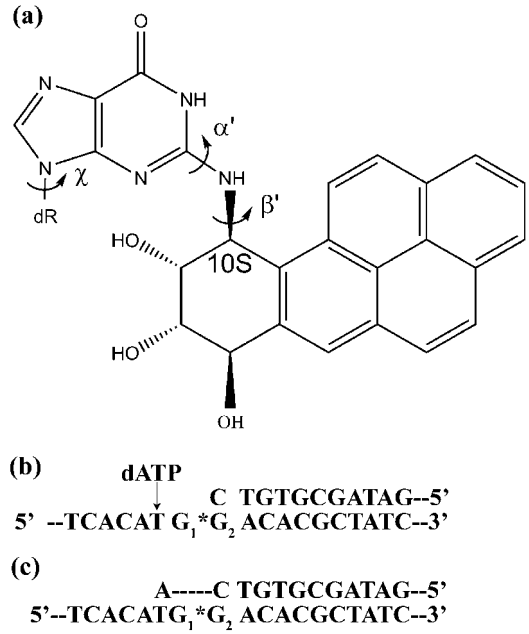

FIGURE 1: (a) Structure of the [BP]G* adduct. Torsion-angle definitions are as follows: χ, O4′−C1′−N9−C8; α', N1−C2−N^2−[BP]C10; β', C2−N^2−[BP]C10−C9. (b) Remodeled DNA sequence in the slippage ternary complex models. (c) Remodeled DNA sequence in the slippage binary complex models.

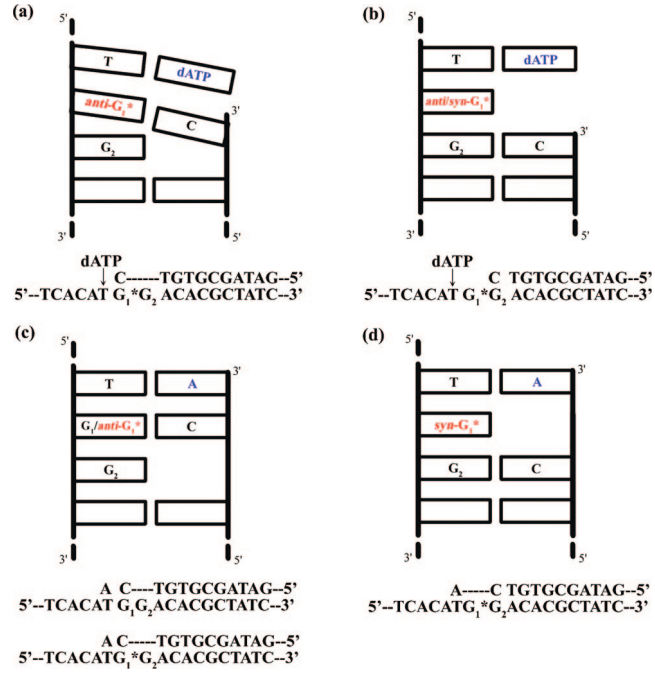

FIGURE 2: Cartoons and DNA sequence schematics showing the (a) 5′- and (b) 3′-slippage patterns in the ternary complex models and the (c) 5′- and (d) 3′-slippage patterns in the binary complex models.

of a Dpo4 ternary complex (*11*) and a binary complex (*15*) reveal that the active site can simultaneously accommodate two templating bases; while the 5′-side templating base is partnered, the base on the 3′ side is skipped (parts a and b of Figure S1 in the Supporting Information). Such slipped structures could lead to a –1 deletion or frameshift mutation in a coding region when the template strand is fully replicated.

Dpo4 has an open pocket on the major groove side of the template strand and a less spacious pocket on the minor groove side and lacks the minor groove binding track that contributes to the high fidelity and processivity of replicative polymerases (*25–29*). In addition to the palm, thumb, and finger domains found in replicative polymerases, Dpo4 has a flexible little-finger domain at the C terminus, which is also called the wrist or polymerase-associated domain (PAD) in other Y-family polymerases (*11, 30, 31*). It has been suggested that this domain plays an important role in accommodating specific types of DNA lesions (*11, 13, 17*) and facilitating DNA translocation (*19*).

The 10*S*(+)-*trans*-*anti*-[BP]-N^2-dG ([BP]G*) adduct (Figure 1a) is a predominant DNA reaction product of (+)-*anti*-BPDE, the highly mutagenic and tumorigenic metabolite of the environmental contaminant benzo[*a*]pyrene (*32–37*). It has been shown that Dpo4 can incorporate all four nucleotides rather promiscuously opposite the [BP]G* adduct in the CG*A sequence context (*38*). Moreover, primer extension experiments reveal that further extension beyond the lesion is generally relatively facile (ref *39* and Oum et al., manuscript in preparation) as compared to the bypass catalyzed by replicative polymerases; the latter often allows for slow nucleotide insertion but strongly inhibits further extension (*40–44*).

We have carried out single-nucleotide insertion studies in Dpo4 with the templating [BP]G* adduct in the $TG_1{*}G_2$ sequence context; this sequence was chosen for its ability to allow for slippage. It differs from the nonslippage-capable CG*A sequence investigated previously (*38*) and thus affords an opportunity to investigate effects of base-sequence context. A significant preference for dATP insertion was observed. These experimental results provided a foundation for molecular modeling and dynamics simulation studies, with the goal of providing a molecular explanation for the experimental observations. We propose that two possible dATP insertion modes contribute to the significant preference for the incorporation of this nucleotide: the dATP can pair with either the T or G_1* in the $TG_1{*}G_2$ sequence, leading to either a −1 deletion or a G:A mismatch mutation, respectively. The dATP insertion opposite the T is favored only when a slippage pattern, which we term 5′ slippage, is adopted in this $TG_1{*}G_2$ repetitive sequence: the dATP pairs with the T, and the unadducted G_2 rather than the lesion G_1*, is skipped entirely (Figure 2a). Such a slippage pattern may be of general importance in sequence contexts where the base 3′ to the lesion is identical to the adducted base.

MATERIALS AND METHODS

Chemicals, Enzymes, and Oligonucleotides. [γ-^{32}P]ATP (3000 Ci/mmol) was purchased from Perkin-Elmer Life Sciences, Inc. (Boston, MA). The dNTPs, dATP, dCTP, dGTP, and dTTP, were purchased from New England Biolabs, Inc. (Beverly, MA). *S. solfataricus* DNA polymerase IV (Dpo4) was kindly provided by Roger Woodgate and Dinshaw Patel. The site-specifically modified 43-mer template oligonucleotide strand, 5′-GAC TAC GTA CTG TCA CAX G*GA CAC GCT ATC TGG CCA GAT CCG C-3′, was synthesized and purified, and the adduct stereochemistry was verified as described earlier (*40*).

Single dNTP Insertion Opposite the Template Lesion Site. The 43-mer template was annealed with a 5′-end ^{32}P-labeled 24-mer primer as shown in Figure 3a. The one-step dNTP

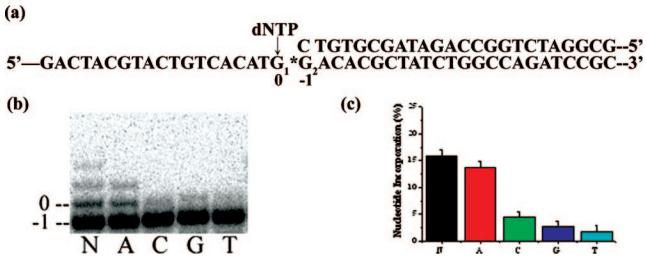

FIGURE 3: Standing-start single-nucleotide incorporation using different 2′-deoxynucleotide triphosphates (dNTP) catalyzed by Dpo4. (a) Sequences of the template and primer strands and numbering scheme. (b) Typical gel electrophoresis patterns of single-step dNTP insertions catalyzed by Dpo4. The dNTP used in each separate experiment is designated by the letters A, C, G, and T. The darkest and lowest band is the 24-nucleotide-long primer strand with its 3′-terminal base positioned opposite G_2, designated as the –1 site, where "0" designates the site of G_1*. The weak upper band represents the 25-mers resulting from the successful incorporation of one nucleotide. The reactions were initiated using 100 μM of each dNTP, 4.5 nM [DNA], and 10 nM Dpo4 at 37 °C for 5 min. (c) Fractions of 24-mers extended.

insertion assays were carried out, and the replication products were visualized and analyzed according to methods described previously (*45*).

Molecular Modeling. The crystal structures of slippage ternary (PDB ID 1JXL) (*11*) and binary (PDB ID 2bq3) (*15*) complexes were used as the starting structures for molecular modeling, with coordinates obtained from the Protein Data Bank (*46*). All molecular modeling was carried out using Insight 2000.1 (Accelrys, Inc., a subsidiary of Pharmacopeia, Inc.).

1. Remodeling the Slippage Ternary Complex. To obtain suitable starting structures for the [BP]G* simulations, we first remodeled the crystal structure (PDB ID 1JXL) (*11*) and carried out MD simulations to find a near reaction-ready snapshot. We removed the ethylene glycol molecule with no biological significance from the crystal. The Ca^{2+} ion, in the position of the nucleotide-binding position, was substituted with a more biologically relevant Mg^{2+} ion. Then, the two Mg^{2+} ions were slightly repositioned, and two water molecules were added to achieve proper octahedral coordination (Figure S2 in the Supporting Information). The DNA sequence in the crystal (Figure S1a in the Supporting Information) was remodeled to that used experimentally (Figure 1b) with 5′-TG_1 in the active site and the primer terminal C pairing with G_2 (Figure S3a in the Supporting Information). Missing hydrogen atoms were added using the LEaP module in AMBER (*47*). We then fully equilibrated this structure and carried out 2.5 ns of MD simulations. During the MD, the primer terminal C, previously paired with G_2 in TG_1G_2, senses the presence of G_1 (the skipped base), moves toward the incoming nucleotide, and pairs with G_1, beginning at ~1.7 ns until the end of the simulation (Figure S3b in the Supporting Information). As the O3′ of the primer terminal C approaches closer to the dATP, it forms two hydrogen bonds with the O5′ and O1α of the dATP; the two hydrogen bonds pull the dATP closer to the primer end (Figure S3c in the Supporting Information). As a result, the Pα−O3′ distance becomes smaller and falls into the near reaction-ready range during this period of the simulation (Figure S3d in the Supporting Information). We selected one snapshot from this period: the structure at 2 ns MD has a Pα−O3′ distance of 3.3 Å, an attack angle of 169.3°, and excellent octahedral Mg^{2+} coordination (Figure S2) (in the original crystal, the Pα−O3′ distance was 4.0 Å and the O3′−Pα−O3α attack angle was 141.7°). In this structure, the primer terminal C pairs simultaneously with both G's in TG_1G_2 through bifurcated hydrogen bonds (Figures S3c, S4a, and S5a in the Supporting Information). We employed this structure to build the initial models for [BP]G*. This structure also provided the initial model for the simulation of the unmodified control.

2. Remodeling the Slippage Binary Complex. For the binary complex (PDB ID 2bq3) (*15*), the DNA sequence in this crystal (Figure S1b in the Supporting Information) was remodeled (Figure 1c) and the missing hydrogen atoms were added using the LEaP module (*47*).

3. Constructing Initial [BP]G Models.* The above remodeled slippage ternary and binary complexes were used to build the initial models for MD simulations. The BP moiety was covalently linked to the N^2 of the templating guanine. We investigated both *anti* and *syn* conformations of the glycosidic torsion angle χ of the BP-adducted dG* (Figure 1a). The torsion angles α′ and β′ at the linkage site between the guanine and the BP (Figure 1a) were rotated at 10° intervals within the low-energy domains (*48*), in combination, to locate conformations with minimal collisions. Around 500 structures were evaluated in each case. For the ternary complex, two *anti*-[BP]G* models and one *syn*-[BP]G* model were located, and for the binary complex, one *anti*-[BP]G* model and one *syn*-[BP]G* model were built. The torsion angles for all initial models are given in Table S1 in the Supporting Information. The remodeled slippage ternary and binary complexes also provided the initial models for the unmodified controls. All initial models are shown in Figures S4 and S5 in the Supporting Information.

MD Simulation Protocol. Partial charges for *anti*/*syn*-[BP]G* and *anti*-dATP were computed previously (*44, 49*). Minimization, equilibration, and production MD were carried out using the same software and protocols as in Xu et al. (*44*), also described in detail in the Supporting Information.

Trajectory Analysis and Stability of the MD Simulations. To obtain ensemble average values for properties of interest, trajectories were collected for all systems and analyzed using the PTRAJ and CARNAL modules of the AMBER package (*47*). For each system, the root-mean-square deviation (rmsd) values of the whole structure and the active site (composed of all of the residues within 5 Å of the nascent base pair) were calculated relative to the first production frame (Figure S6 in the Supporting Information). We found that all systems are stable from 1.0 to 2.5 ns. The following analyses are based on these ranges. All structural figures were prepared using PyMOL (*50*).

RESULTS

Standing-Start Single-Nucleotide Insertion Assays Reveal Significant Preferential dATP Insertion. The "standing-start" insertion experiment is defined in Figure 3a. In this arrangement, the modified base G_1* is the next to be replicated by dNTP incorporation. Among the four nucleotides, dATP was most efficiently incorporated in the sequence context that we investigated here (parts b and c of Figure 3). We hypothesize that this preference can be explained by a slippage mechanism

involving pairing of dATP with the T on the 5′ side of the G_1* lesion in the TG_1*G_2 sequence context (Figure 1b), in addition to dATP mispairing with G_1* (ref *38* and Xu et al., manuscript in preparation), the next to be replicated template base. To investigate the feasibility of this slippage, we conducted a molecular modeling and dynamics simulation study.

Molecular Modeling and Dynamics Simulations. For the MD simulations (see the Materials and Methods), we considered modified ternary and binary complexes and their respective unmodified controls. In the ternary complex, the primer 3′-terminal base is C and a dATP is about to be incorporated into the 3′ end of the primer strand. In the binary complex, this incorporation has occurred, the primer 3′-terminal base is therefore A, and there is no dNTP present. For both ternary and binary complexes, we constructed initial models with either *anti*- or *syn*-[BP]G* glycosidic torsion-angle orientations at the modified dG* residue for evaluation (parts a−g of Figures S4 and S5 in the Supporting Information). These models were analyzed to determine if bypass of the lesion involving the hypothetical slippage mechanism is feasible and can lead to the next stage of DNA replication to produce a −1 deletion mutation. The structures, after MD, are shown in Figure 4 and Figures S7 and S8 in the Supporting Information, and analyses of the trajectory ensembles are provided in Tables S2−S5 and Figures S9 and S10 in the Supporting Information.

1. Ternary Complex Models Show a 5′-Slippage Pattern with the Primer 3′-Terminal C Pairing with G_1 in the TG_1*G_2 Sequence Context.* All of the ternary complex models have 5′-TG_1 (unmodified) or 5′-TG_1* (modified) dinucleotide sequences in the active site, with the incoming dATP paired with the T (Figure 1b and parts a−d of Figures S4 and S5 in the Supporting Information). We found that when the BP-modified dG_1* adopts the *anti* conformation, the primer 3′-terminal C can pair with either G_1* (5′ slippage) or G_2 (3′ slippage) through Watson–Crick hydrogen bonding (parts a and b of Figure 2). However, with the dG_1* *syn*, this C can only pair with G_2 (3′ slippage) because the *syn*-dG_1* does not allow Watson–Crick hydrogen bonding (Figure 2b). The 5′-slippage pattern favors dATP insertion opposite the T on the 5′ side of the adduct, while the 3′-slippage pattern disfavors it (Table 1).

(A) The Unmodified Control Demonstrates a Generally Near Reaction-Ready Active Site. The structure described in the Materials and Methods, which evolved through MD based on the crystal structure (PDB ID 1JXL) (*11*), was employed for the simulation of the unmodified control (Figures S4a and S5a in the Supporting Information). In this initial model, the primer 3′-terminal C pairs simultaneously with both G_1 and G_2 through bifurcated hydrogen bonds. However, during the simulation, this C position fluctuates, to pair alternately with G_1 (Figure 2a) (occupancies 46.4, 47.4, and 44.8%) and G_2 (Figure 2b) (occupancies 86.6, 57.1, and 50.3%) (Table S2 in the Supporting Information). The two hydrogen bonds in the nascent T:dATP pair are intact throughout the dynamics simulation (occupancies 99.3 and 95.7%) (Table S2 in the Supporting Information). Hydrogen bond occupancies are the percent of time during the stable region of the MD trajectory (1.0–2.5 ns) that the hydrogen bond is present according to the following criteria: 3.3 Å between heavy atoms (donor and acceptor) and a hydrogen bonding donor–hydrogen–acceptor angle of 135°. The dATP is stabilized by hydrogen bonds with the amino acid residues

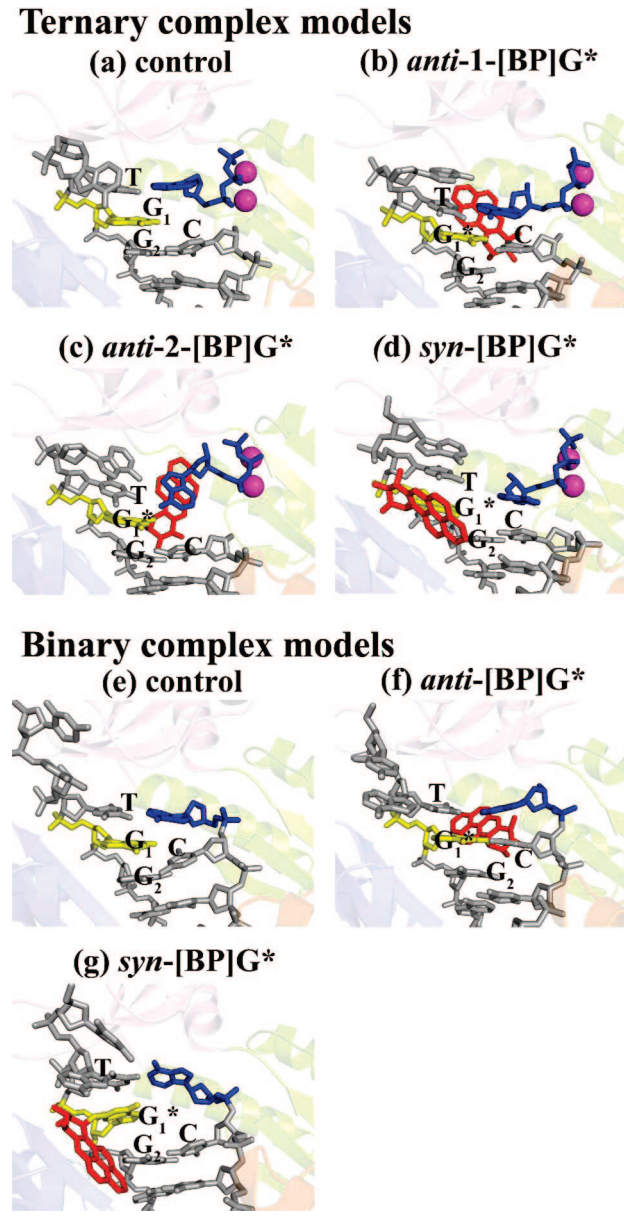

FIGURE 4: Simulated systems after 2.5 ns MD. The polymerase is shown in a ribbon representation. Color code: orange, thumb domain; green, palm domain; light pink, finger domain; blue, little-finger domain; gray, primer/template DNA strand; magenta, Mg^{2+} ions (sphere representation); yellow, unmodified or modified dG; red, BP moiety; blue, dATP/dA. The bases T, G_1/G_1*, G_2, and C are indicated in each system.

Tyr-12, Thr-45, and Arg-51 (Table S3 in the Supporting Information). The key structural properties at the active site in our unmodified control, namely, the C1′−C1′ distance in the nascent base pair, the Pα−O3′ alignment, and the distance between the two Mg^{2+} ions and their coordination, closely resemble those in a recent polymerase crystal structure with a well-resolved active site (*51*). Specifically, the C1′−C1′ distance in the nascent T:dATP pair has an ensemble average value of 10.6 ± 0.4 Å and samples the 9.8−11.8 Å range with an occupancy of 99.3%. The Pα−O3′ distance (ensemble average 3.7 ± 0.6 Å) achieves the near reaction-ready range (3.1–3.5 Å) with a frequency of 56.0%, and the O3′−Pα−O3α angle (ensemble average 160.5 ± 8.1°) samples the in-line attack range (160−180°) for 54.7% of the time. The Mg^{2+}A−Mg^{2+}B distance has an average

Table 1: Structural Properties of Models

slippage ternary complexes		
models	positioning of the primer 3′-terminal C	Pα−O3′ alignment
anti-1-[BP]G*	G_1* pairing (5′ slippage)	good
anti-2-[BP]G*	G_2 pairing (3′ slippage)	poor
syn-[BP]G*	G_2 pairing (3′ slippage)	poor

slippage binary complexes		
models	positioning of the C on the 5′ side of the primer 3′-terminal A	positioning of the primer 3′-terminal A
anti-[BP]G*	G_1* pairing (5′ slippage)	stably paired with the template T
syn-[BP]G*	G_2 pairing (3′ slippage)	unstable during the MD and repositions itself to interfere with subsequent nucleotide binding

value of 3.6 ± 0.1 Å (Table S4 in the Supporting Information). The octahedral coordination of the two Mg^{2+} ions remains unperturbed throughout MD (Table S5 in the Supporting Information). Altogether, the structural properties appear normal in this unmodified control.

(B) The anti-[BP]G Minor Groove Models Reveal a 5′-Slippage Pattern That Favors dATP Insertion Opposite the T.* Because both *anti*-dG_1* and dG_2 permit Watson–Crick hydrogen bonding with the primer 3′-terminal C, we constructed two *anti*-[BP]G* initial models: *anti*-1-[BP]G* [the C pairs with G_1* (Figures S4b and S5b in the Supporting Information)] and *anti*-2-[BP]G* [the C pairs with G_2 (Figures S4c and S5c in the Supporting Information)]. During MD, the *anti*-1-[BP]G* system retains the G_1*-pairing (5′ slippage) pattern (Figures 2a and 4b and Figures S7b and S8b in the Supporting Information) and the *anti*-2-[BP]G* system preserves the G_2-pairing (3′ slippage) pattern (Figures 2b and 4c and Figures S7c and S8c in the Supporting Information). This differs from the unmodified control, in which the C position fluctuates between the unmodified G_1 and G_2. The BP moiety constitutes a barrier that keeps the primer 3′-terminal C from moving between the two G's in TG_1*G_2 and thus prevents interchange between the two slippage patterns (parts b and c of Figure 4 and parts b and c of Figures S7 and S8 in the Supporting Information). The 5′-slippage pattern supports a good Pα−O3′ alignment and thus favors dATP insertion opposite the T on the 5′ side of the adduct; however, the 3′-slippage pattern shows a poor Pα−O3′ alignment and thus disfavors dATP insertion opposite the T (Table 1).

Specifically, in the *anti*-1-[BP]G* system, the primer 3′-terminal C predominantly pairs with G_1* (occupancies 96.5, 89.9, and 84.9%) and very rarely pairs with G_2 during the MD simulation (Table S2 in the Supporting Information). The structural properties important for polymerase function are near normal. The two hydrogen bonds between the templating T and the incoming dATP are unperturbed throughout the simulation (occupancies 96.9 and 88.6%) (Table S2 in the Supporting Information). Two amino acids, Tyr-12 and Lys-159, hydrogen bond with the O3′, O1β, and O1γ of the dATP (Table S3 in the Supporting Information). The ensemble average of the (T) C1′−(dATP) C1′ distance (10.6 ± 0.3 Å) is similar to that of the control and samples the 9.8−11.8 Å range with a frequency of 99.8%. The Pα−O3′ distance (ensemble average 3.8 ± 0.8 Å) samples the near reaction-ready range with an occupancy of 49.5%, and the O3′−Pα−O3α angle (ensemble average 156.5 ± 8.3°) achieves the in-line attack range (160−180°) during 35.1% of the simulation time. The distance between the two Mg^{2+} ions is normal compared to the control (Table S4 in the Supporting Information). Only one of the interactions coordinating the Mg^{2+} ions is broken, with the distance between the nucleotide-binding Mg^{2+} and the O of a coordinating water significantly increased (Table S5 in the Supporting Information).

However, in the *anti*-2-[BP]G* system, the primer 3′-terminal C primarily hydrogen bonds with G_2 (occupancies 99.6, 97.0, and 85.4%) and is not observed to pair with G_1 even transiently during MD (Table S2 in the Supporting Information). The dATP is stabilized by hydrogen bonds with three amino acid residues, Lys-159, Thr-45, and Arg-51 (Table S3 in the Supporting Information). Although the distance between the two Mg^{2+} ions and their coordinations are preserved well in this system (Tables S4 and S5 in the Supporting Information), other important structural properties are severely disrupted. The two hydrogen bonds in the nascent T:dATP pair are essentially broken (Table S2 in the Supporting Information). The C1′−C1′ distance in the T:dATP pair is significantly increased (ensemble average 12.0 ± 0.3 Å) and samples the 9.8−11.8 Å range with a low frequency of 25.1% (Table S4 in the Supporting Information). The Pα−O3′ distance has an ensemble average value of 5.8 ± 0.6 Å and achieves the near reaction-ready range (3.1−3.5 Å) with a negligible occupancy of 0.4% (Table S4 in the Supporting Information). The O3′−Pα−O3α angle (ensemble average 139.5 ± 11.1°) samples the in-line attack range (160−180°) with a very low frequency of 3.0% (Table S4 in the Supporting Information).

Overall, when the BP-modified dG_1* adopts the *anti* conformation, the primer 3′-terminal C pairs with either G_1* (5′ slippage) (Figure 2a) or G_2 (3′ slippage) (Figure 2b), with the 5′-slippage pattern favoring dATP insertion opposite the T base on the 5′ side of the adduct and the 3′-slippage pattern disfavoring it (Table 1).

(C) The syn-[BP]G Major Groove Model Shows a 3′-Slippage Pattern, Which Disfavors dATP Insertion Opposite the T.* In the initial model, there is no hydrogen bond between the primer 3′-terminal C and G_1* (Figures S4d and S5d in the Supporting Information). During the MD simulation, this C remains paired with G_2 (3′ slippage) (Figure 2b). The structure has poor Pα−O3′ alignment and therefore does not support dATP insertion opposite the T 5′ to the adduct (Table 1). Specifically, during the simulation, the primer 3′-terminal C predominantly pairs with G_2 (occupancies 99.5, 100.0, and 98.4%) (Table S2 in the Supporting Information) and is never observed to hydrogen bond with G_1*. Although the (T)

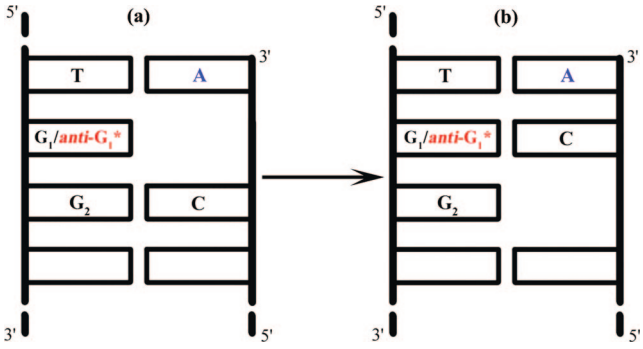

FIGURE 5: Repositioning of the C on the 5′ side of the inserted A in the *anti*-[BP]G* and unmodified binary complex models. (a) Initial state where the C pairs with G_2 (3′ slippage). (b) C moves to pair with G_1/G_1* (5′ slippage) during equilibration and primarily stays there throughout MD.

C1′−(dATP) C1′ distance, in-line attack angle, and the distance between the two Mg^{2+} ions appear near normal compared to the unmodified control, the Pα−O3′ distance is large (ensemble average 5.8 ± 0.6 Å) and never samples the near reaction-ready range (Table S4 in the Supporting Information). In addition, the dATP drifts away from its normal position and moves closer to the primer 3′-terminal C (Figure 4d and Figures S7d and S8d in the Supporting Information). The two hydrogen bonds in the nascent T:dATP pair are essentially broken (Table S2 in the Supporting Information). The interaction between the nucleotide-binding Mg^{2+} ion and the water molecule is disrupted, while all of the other 11 coordinating interactions are preserved (Table S5 in the Supporting Information). Altogether, although the BP is placed on the more open major groove side of the modified template when the dG* is *syn*, dATP insertion opposite the T on the 5′ side of the adduct is disfavored because the primer 3′-terminal C pairs only with G_2 (3′ slippage), in a nonproductive alignment (Figure 2b).

2. Binary Complex Models Maintain the 5′-Slippage Pattern. All of the binary complex models have the primer 3′-terminal A pairing with the template T in the TG_1G_2 (unmodified) or TG_1*G_2 (modified) cases and the adjacent C on the 5′ side of this A pairing with G_2, with G_1 (unmodified) or G_1* (modified) unpaired (Figure 1c and parts e−g of Figures S4 and S5 in the Supporting Information). The MD simulations reveal that a G_1*-pairing (5′ slippage) pattern develops in the *anti*-[BP]G* system (Figure 2c) and a G_2-pairing (3′ slippage) pattern persists in the *syn*-[BP]G* case (Figure 2d). The G_1*-pairing (5′ slippage) pattern supports a more stable structure that allows for the propagation of slippage to the next step of DNA replication (Table 1).

(A) The Unmodified Control Shows Generally Unperturbed Structural Properties. The C in the primer strand, which is on the 5′ side of the 3′-terminal A, was paired with G_2 in the TG_1G_2 initial model (Figure 5a and Figures S4e and S5e in the Supporting Information); however, this C repositions itself during the course of the dynamics simulation, so that it hydrogen bonds mainly with G_1 (occupancies 99.5, 97.8, and 77.3%) and pairs with the G_2 only occasionally (occupancies 11.2, 28.4, and 28.9%) (Table S2 in the Supporting Information, Figures 4e and 5b, and Figures S7e and S8e in the Supporting Information). The two Watson–Crick hydrogen bonds in the primer terminal T:A pair are intact (occupancies 94.0 and 98.3%) (Table S2 in the Supporting Information). The C1′−C1′ distance in the primer terminal base pair has an average value of 10.9 ± 0.3 Å and samples the 9.8−11.8 Å range with a frequency of 99.7% (Table S4 in the Supporting Information). Therefore, this structure appears normal during the MD simulation.

(B) The anti-[BP]G Minor Groove Model Reveals a 5′-Slippage Pattern That Favors Propagation of Slippage to the Next Stage of DNA Replication.* The C in the primer strand on the 5′ side of the 3′-terminal A, initially paired with G_2 (3′ slippage) in TG_1*G_2 (Figure 5a and Figures S4f and S5f in the Supporting Information), gradually approaches G_1* during the simulation. This C then pairs predominantly with G_1* (5′ slippage) (occupancies 100.0, 93.2, and 84.1%) and only hydrogen bonds with G_2 with negligible occupancies during the MD simulation (Table S2 in the Supporting Information, Figures 4f and 5b, and Figures S7f and S8f in the Supporting Information). This is in contrast to the corresponding *anti*-[BP]G* ternary complex systems, in which the C remains sequestered at its original position (parts b and c of Figure 4 and parts b and c of Figures S7 and S8 in the Supporting Information). The BP moiety can reorient itself more freely in the binary complex than in the ternary complex, thus allowing repositioning of the C at the beginning of the simulation. As the C begins to pair with G_1*, the stretching distortion in the DNA backbone between the C and the 3′-terminal A in the primer strand is alleviated and the stacking interactions between the two bases is strengthened (Figure 4f and Figures S7f and S8f in the Supporting Information). As a result, both the C and the 3′-terminal A remain stable throughout the simulation. The C remains paired with G_1*. The two hydrogen bonds in the primer terminal T:A pair remain essentially unperturbed (occupancies 74.3 and 96.3%) (Table S2 in the Supporting Information). The C1′−C1′ distance in the T:A base pair is slightly increased (ensemble average 11.2 ± 0.2 Å) as compared to the control but nevertheless samples the 9.8−11.8 Å range with a frequency of 99.3% (Table S4 in the Supporting Information). In summary, a G_1*-pairing (5′ slippage) pattern (Figure 2c) is achieved during the MD of this system. The whole structure appears near normal and favorable for further extension in the presence of a skipped template base. Therefore, the −1 deletion appears likely to be propagated to the next stage of DNA replication.

(C) The syn-[BP]G Major Groove Model Shows a 3′-Slippage Pattern Not Favorable for Propagation of Slippage to the Next Stage of DNA Replication.* As described above, the *syn*-[BP]G* ternary complex does not favor dATP insertion opposite the template T in the TG_1*G_2 sequence context. However, a *syn*-[BP]G* binary complex with A incorporated opposite the T in TG_1*G_2 could result from a different extension mechanism: insertion of the mismatched dATP opposite the adduct, followed by a slip of this primer 3′-terminal A to pair with the T. Consequently, we studied the properties of a *syn*-[BP]G* binary complex. In this system, the C on the 5′ side of the primer 3′-terminal A is hydrogen-bonded with G_2 (3′ slippage) in the initial model (Figures S4g and S5g in the Supporting Information) and remains paired with G_2 (3′ slippage) during the simulation (occupancies 97.1, 99.1, and 93.9%) (Figure 2d). It never forms hydrogen bonds with G_1* (Table S2 in the Supporting

Information). The primer 3′-terminal A with no base-stacking neighbor in contact on its 5′ side is not stable during the MD and repositions itself to interfere with subsequent nucleotide binding (Figure 4g and Figures S7g and S8g in the Supporting Information). The two hydrogen bonds in the primer terminal T:A base pair are disturbed (both occupancies are decreased by ~40% as compared to the control) (Table S2 in the Supporting Information), and the C1′−C1′ distance of this base pair samples the 9.8−11.8 Å range with a frequency of 88.9%, more than 10% lower than in the case of the unmodified control (Table S4 in the Supporting Information). Overall, the C on the 5′ side of the primer 3′-terminal A remains G_2-paired with 3′ slippage (Figure 2d). Several structural properties are disrupted, and further extension with slippage is disfavored.

DISCUSSION

In the present study, we have performed standing-start single-dNTP insertion assays with the [BP]G* adduct as the next to be replicated template base in a 5′-TG_1*G_2-3′ sequence context and have detected a significant preference for dATP insertion (Figure 3). We hypothesized that this preference results from a slip of dATP to pair with the template base T on the 5′ side of G_1* (Figure 1b), in addition to dATP mispairing with the adduct. Pairing of dATP with [BP]G* has been previously shown, through MD simulations from our group, to be readily accommodated in the Dpo4 active site (*38*). To investigate the structural feasibility of slippage, MD simulations were carried out for two *anti*-[BP]G* and one *syn*-[BP]G* models based on the crystal structure of the slippage ternary complex. In addition, two binary complex models, one *anti*-[BP]G* and one *syn*-[BP]G*, were similarly investigated to determine if slippage is stable following dATP incorporation opposite the template base T and thus can be propagated to the next stage of DNA replication.

Our results show two possible slippage patterns, G_1* pairing (5′ slippage) and G_2 pairing (3′ slippage) (parts a and b of Figure 2). The 5′-slippage pattern favors dATP insertion opposite the T on the 5′ side of the adduct as well as further primer extension beyond this T:A base pair, but the 3′-slippage pattern does not (Table 1). As the 3′-slippage pattern is adopted, the dATP or dA after the nucleotidyl reaction could instead pair with the adducted guanine G_1* itself. Insertion of a mismatched A opposite the [BP]G* has been observed in Dpo4 experimentally with DNA sequences that are not favorable for slippage (*38*). Mismatched *syn*-dG*:*anti*-dATP/dA and *anti*-dG*:*syn*-dATP/dA base pairs can be well-accommodated at the active-site region of Dpo4 during the dNTP insertion and subsequent extension steps (ref *38* and Xu et al., manuscript in preparation). Therefore, the dATP can be incorporated by Dpo4 with and without slippage in the TG_1*G_2 sequence context. Further extension would produce either a −1 deletion or a G:A mismatch mutation. However, the other three dNTPs would be predominantly inserted only opposite the adduct. Misinsertion of a dCTP, dGTP, or dTTP opposite the T on the 5′ side of G_1*, which would lead to a simultaneous mismatch and deletion mutation, would be much less likely. This explains why dATP is preferred over the other three nucleotides in the single dNTP insertion assays (Figure 3).

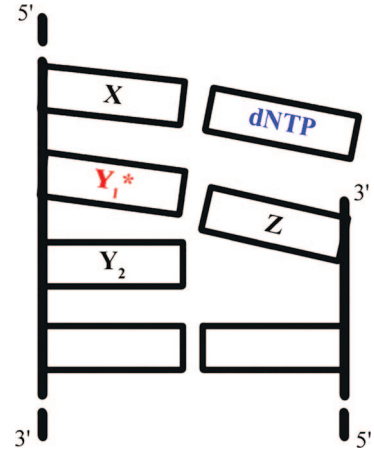

FIGURE 6: 5′-Slippage pattern which may be applicable to repetitive sequence context, 5′-XY_1*Y_2-3′, with dNTP being complementary to X. Z is the primer 3′-terminal base, which can alternately form Watson–Crick hydrogen bonds with Y_1* or Y_2.

The 5′-slippage pattern has not, to our knowledge, been previously characterized. The TG_1*G_2 sequence contains two G bases, which can alternately form Watson–Crick pairs with the same C partner base on the primer strand. These alternative pairing patterns are not interchangeable because of steric impediment by the bulky BP ring system within the polymerase ternary complex. Other repetitive sequence contexts, 5′-XY_1*Y_2-3′, may allow for a similar mechanism, with dNTP being complementary to X (Figure 6). Eventually, a −1 deletion could occur. In contrast, for sequences that do not support the 5′-slippage pattern, a −1 deletion could occur via a bulging out of the adducted base on the template strand, as suggested by a recent Dpo4 crystal structure with a bulged-out [BP]G* at the extension step (*20*).

CONCLUSIONS

In the current work, we have rationalized, through molecular modeling and dynamics simulations, the preference for dATP insertion in standing-start single-dNTP insertion assays, with the [BP]G* as the base next to be replicated in a TG_1*G_2 sequence context. Modeling studies suggest that this preference is due to dATP insertion opposite both the T and G_1* template bases, to produce a −1 deletion or a G:A mismatch mutation. The dATP insertion opposite T involves a 5′-slippage pattern with the base on the 3′ side of the adduct, instead of the adduct, being skipped. This requires that the skipped base is the same as the adducted one. Such a mechanism may be applicable to other sequence contexts with an analogous repetitive theme; it could be relevant to other DinB family polymerases, including the slippage prone human pol κ (*52*), whose structure, while possessing an additional N-clasp domain (PDB ID 2OH2) (*53*), resembles significantly that of Dpo4. Our 5′-slippage mechanism differs from the one described by Bauer et al. (*20*), based on crystallographic and primer extension studies, where the damaged base is in a nonrepetitive sequence context; in that case, it is the adducted base that is skipped. The relevance of these types of mechanisms to in vivo mutagenesis is a topic of considerable current interest (*54*).

ACKNOWLEDGMENT

Computational resources supported by the National Science Foundation (NSF) Partnerships for Advanced Computational Infrastructure are gratefully acknowledged.

SUPPORTING INFORMATION AVAILABLE

Details of MD simulation protocols, torsion angles of [BP]G* for all initial models, and detailed analyses of trajectory ensembles. This material is available free of charge via the Internet at http://pubs.acs.org.

REFERENCES

1. Pages, V., and Fuchs, R. P. (2002) How DNA lesions are turned into mutations within cells. *Oncogene 21*, 8957–8966.
2. Friedberg, E. C., Lehmann, A. R., and Fuchs, R. P. (2005) Trading places: How do DNA polymerases switch during translesion DNA synthesis. *Mol. Cell 18*, 499–505.
3. Plosky, B. S., and Woodgate, R. (2004) Switching from high-fidelity replicases to low-fidelity lesion-bypass polymerases. *Curr. Opin. Genet. Dev. 14*, 113–119.
4. McCulloch, S. D., Kokoska, R. J., Chilkova, O., Welch, C. M., Johansson, E., Burgers, P. M., and Kunkel, T. A. (2004) Enzymatic switching for efficient and accurate translesion DNA replication. *Nucleic Acids Res. 32*, 4665–4675.
5. Lehmann, A. R. (2006) Translesion synthesis in mammalian cells. *Exp. Cell Res. 312*, 2673–2676.
6. Prakash, S., Johnson, R. E., and Prakash, L. (2005) Eukaryotic translesion synthesis DNA polymerases: Specificity of structure and function. *Annu. Rev. Biochem. 74*, 317–353.
7. Guengerich, F. P. (2006) Interactions of carcinogen-bound DNA with individual DNA polymerases. *Chem. Rev. 106*, 420–452.
8. Boudsocq, F., Iwai, S., Hanaoka, F., and Woodgate, R. (2001) *Sulfolobus solfataricus* P2 DNA polymerase IV (Dpo4): An archaeal DinB-like DNA polymerase with lesion-bypass properties akin to eukaryotic polη. *Nucleic Acids Res. 29*, 4607–4616.
9. Ohashi, E., Ogi, T., Kusumoto, R., Iwai, S., Masutani, C., Hanaoka, F., and Ohmori, H. (2000) Error-prone bypass of certain DNA lesions by the human DNA polymerase κ. *Genes Dev. 14*, 1589–1594.
10. Ling, H., Sayer, J. M., Plosky, B. S., Yagi, H., Boudsocq, F., Woodgate, R., Jerina, D. M., and Yang, W. (2004) Crystal structure of a benzo[*a*]pyrene diol epoxide adduct in a ternary complex with a DNA polymerase. *Proc. Natl. Acad. Sci. U.S.A. 101*, 2265–2269.
11. Ling, H., Boudsocq, F., Woodgate, R., and Yang, W. (2001) Crystal structure of a Y-family DNA polymerase in action: A mechanism for error-prone and lesion-bypass replication. *Cell 107*, 91–102.
12. Ling, H., Boudsocq, F., Plosky, B. S., Woodgate, R., and Yang, W. (2003) Replication of a *cis-syn* thymine dimer at atomic resolution. *Nature 424*, 1083–1087.
13. Ling, H., Boudsocq, F., Woodgate, R., and Yang, W. (2004) Snapshots of replication through an abasic lesion; structural basis for base substitutions and frameshifts. *Mol. Cell 13*, 751–762.
14. Vaisman, A., Ling, H., Woodgate, R., and Yang, W. (2005) Fidelity of Dpo4: Effect of metal ions, nucleotide selection and pyrophosphorolysis. *EMBO J. 24*, 2957–2967.
15. Zang, H., Goodenough, A. K., Choi, J. Y., Irimia, A., Loukachevitch, L. V., Kozekov, I. D., Angel, K. C., Rizzo, C. J., Egli, M., and Guengerich, F. P. (2005) DNA adduct bypass polymerization by *Sulfolobus solfataricus* DNA polymerase Dpo4: Analysis and crystal structures of multiple base pair substitution and frameshift products with the adduct 1,N^2-ethenoguanine. *J. Biol. Chem. 280*, 29750–29764.
16. Trincao, J., Johnson, R. E., Wolfle, W. T., Escalante, C. R., Prakash, S., Prakash, L., and Aggarwal, A. K. (2004) Dpo4 is hindered in extending a G•T mismatch by a reverse wobble. *Nat. Struct. Mol. Biol. 11*, 457–462.
17. Boudsocq, F., Kokoska, R. J., Plosky, B. S., Vaisman, A., Ling, H., Kunkel, T. A., Yang, W., and Woodgate, R. (2004) Investigating the role of the little finger domain of Y-family DNA polymerases in low fidelity synthesis and translesion replication. *J. Biol. Chem. 279*, 32932–32940.
18. Zang, H., Irimia, A., Choi, J. Y., Angel, K. C., Loukachevitch, L. V., Egli, M., and Guengerich, F. P. (2006) Efficient and high fidelity incorporation of dCTP opposite 7,8-dihydro-8-oxodeoxyguanosine by *Sulfolobus solfataricus* DNA polymerase Dpo4. *J. Biol. Chem. 281*, 2358–2372.
19. Rechkoblit, O., Malinina, L., Cheng, Y., Kuryavyi, V., Broyde, S., Geacintov, N. E., and Patel, D. J. (2006) Stepwise translocation of Dpo4 polymerase during error-free bypass of an oxoG lesion. *PLoS Biol. 4*, 1–18.
20. Bauer, J., Xing, G., Yagi, H., Sayer, J. M., Jerina, D. M., and Ling, H. (2007) A structural gap in a Y-family DNA polymerase supports mutagenic bypass of a major benzo[*a*]pyrene adduct through template misalignment, *Proc. Natl. Acad. Sci. U.S.A. 104*, 14905–14910.
21. Beard, W. A., and Wilson, S. H. (1998) Structural insights into DNA polymerase β fidelity: Hold tight if you want it right. *Chem. Biol. 5*, R7–R13.
22. Frieden, M., Pedroso, E., and Kool, E. T. (1999) Tightening the belt on polymerases: Evaluating the physical constraints on enzyme substrate size. *Angew. Chem., Int. Ed. 38*, 3654–3657.
23. Sawaya, M. R., Prasad, R., Wilson, S. H., Kraut, J., and Pelletier, H. (1997) Crystal structures of human DNA polymerase β complexed with gapped and nicked DNA: Evidence for an induced fit mechanism. *Biochemistry 36*, 11205–11215.
24. Wong, I., Patel, S. S., and Johnson, K. A. (1991) An induced-fit kinetic mechanism for DNA replication fidelity: Direct measurement by single-turnover kinetics. *Biochemistry 30*, 526–537.
25. Beard, W. A., Bebenek, K., Darden, T. A., Li, L., Prasad, R., Kunkel, T. A., and Wilson, S. H. (1998) Vertical-scanning mutagenesis of a critical tryptophan in the minor groove binding track of HIV-1 reverse transcriptase. Molecular nature of polymerase−nucleic acid interactions. *J. Biol. Chem. 273*, 30435–30442.
26. Bebenek, K., Beard, W. A., Darden, T. A., Li, L., Prasad, R., Luton, B. A., Gorenstein, D. G., Wilson, S. H., and Kunkel, T. A. (1997) A minor groove binding track in reverse transcriptase. *Nat. Struct. Biol. 4*, 194–197.
27. Latham, G. J., Forgacs, E., Beard, W. A., Prasad, R., Bebenek, K., Kunkel, T. A., Wilson, S. H., and Lloyd, R. S. (2000) Vertical-scanning mutagenesis of a critical tryptophan in the "minor groove binding track" of HIV-1 reverse transcriptase. Major groove DNA adducts identify specific protein interactions in the minor groove. *J. Biol. Chem. 275*, 15025–15033.
28. Morales, J., and Kool, E. T. (1999) Minor groove interactions between polymerase and DNA: More essential to replication than Watson−Crick hydrogen bonds. *J. Am. Chem. Soc. 121*, 2323–2324.
29. Polesky, A. H., Dahlberg, M. E., Benkovic, S. J., Grindley, N. D., and Joyce, C. M. (1992) Side chains involved in catalysis of the polymerase reaction of DNA polymerase I from *Escherichia coli*. *J. Biol. Chem. 267*, 8417–8428.
30. Silvian, L. F., Toth, E. A., Pham, P., Goodman, M. F., and Ellenberger, T. (2001) Crystal structure of a DinB family error-prone DNA polymerase from *Sulfolobus solfataricus*. *Nat. Struct. Biol. 8*, 984–989.
31. Trincao, J., Johnson, R. E., Escalante, C. R., Prakash, S., Prakash, L., and Aggarwal, A. K. (2001) Structure of the catalytic core of *S. cerevisiae* DNA polymerase η: Implications for translesion DNA synthesis. *Mol. Cell 8*, 417–426.
32. Conney, A. H. (1982) Induction of microsomal enzymes by foreign chemicals and carcinogenesis by polycyclic aromatic hydrocarbons: G. H. A. Clowes Memorial Lecture. *Cancer Res. 42*, 4875–4917.
33. Buening, M. K., Wislocki, P. G., Levin, W., Yagi, H., Thakker, D. R., Akagi, H., Koreeda, M., Jerina, D. M., and Conney, A. H. (1978) Tumorigenicity of the optical enantiomers of the diastereomeric benzo[*a*]pyrene 7,8-diol-9,10-epoxides in newborn mice: Exceptional activity of (+)-7β,8α-dihydroxy-9α,10α-epoxy-7,8,9,10-tetrahydrobenzo[*a*]pyrene. *Proc. Natl. Acad. Sci. U.S.A. 75*, 5358–5361.
34. Szeliga, J., and Dipple, A. (1998) DNA adduct formation by polycyclic aromatic hydrocarbon dihydrodiol epoxides. *Chem. Res. Toxicol. 11*, 1–11.
35. Cheng, S. C., Hilton, B. D., Roman, J. M., and Dipple, A. (1989) DNA adducts from carcinogenic and noncarcinogenic enantiomers of benzo[*a*]pyrene dihydrodiol epoxide. *Chem. Res. Toxicol. 2*, 334–340.
36. Geacintov, N. E., Cosman, M., Hingerty, B. E., Amin, S., Broyde, S., and Patel, D. J. (1997) NMR solution structures of stereoisometric covalent polycyclic aromatic carcinogen−DNA adduct: Principles, patterns, and diversity. *Chem. Res. Toxicol. 10*, 111–146.

37. Meehan, T., and Straub, K. (1979) Double-stranded DNA sterose-lectively binds benzo[*a*]pyrene diol epoxides. *Nature 277*, 410–412.
38. Perlow-Poehnelt, R. A., Likhterov, I., Scicchitano, D. A., Geacintov, N. E., and Broyde, S. (2004) The spacious active site of a Y-family DNA polymerase facilitates promiscuous nucleotide incorporation opposite a bulky carcinogen−DNA adduct: Elucidating the structure−function relationship through experimental and computational approaches. *J. Biol. Chem. 279*, 36951–36961.
39. Oum, L. (2007) *Base-Sequence and Temperature Effects on in Vitro Studies of Translesion Synthesis past anti-BPDE-N^2-dG Adducts*, Chemistry Department, New York University, New York.
40. Zhuang, P., Kolbanovskiy, A., Amin, S., and Geacintov, N. E. (2001) Base sequence dependence of in vitro translesional DNA replication past a bulky lesion catalyzed by the exo-Klenow fragment of Pol I. *Biochemistry 40*, 6660–6669.
41. Hruszkewycz, A. M., Canella, K. A., Peltonen, K., Kotrappa, L., and Dipple, A. (1992) DNA polymerase action on benzo-[*a*]pyrene−DNA adducts. *Carcinogenesis 13*, 2347–2352.
42. Lipinski, L. J., Ross, H. L., Zajc, B., Sayer, J. M., Jerina, D. M., and Dipple, A. (1998) Effect of single benzo[*a*]pyrene diol epoxide-deoxyguanosine adducts on the action of DNA polymerases in vitro. *Int. J. Oncol. 13*, 269–273.
43. Shibutani, S., Margulis, L. A., Geacintov, N. E., and Grollman, A. P. (1993) Translesional synthesis on a DNA template containing a single stereoisomer of dG-(+)- or dG-(−)-*anti*-BPDE (7,8-dihydroxy-anti-9,10-epoxy-7,8,9,10-tetrahydrobenzo[*a*]pyrene). *Biochemistry 32*, 7531–7541.
44. Xu, P., Oum, L., Beese, L. S., Geacintov, N. E., and Broyde, S. (2007) Following an environmental carcinogen N^2-dG adduct through replication: Elucidating blockage and bypass in a high-fidelity DNA polymerase, *Nucleic Acids Res.*, *35*, 4275–4288.
45. Huang, X., Kolbanovskiy, A., Wu, X., Zhang, Y., Wang, Z., Zhuang, P., Amin, S., and Geacintov, N. E. (2003) Effects of base sequence context on translesion synthesis past a bulky (+)-*trans*-*anti*-B[*a*]P-N^2-dG lesion catalyzed by the Y-family polymerase pol κ. *Biochemistry 42*, 2456–2466.
46. Berman, H. M., Westbrook, J., Feng, Z., Gilliland, G., Bhat, T. N., Weissig, H., Shindyalov, I. N., and Bourne, P. E. (2000) The Protein Data Bank. *Nucleic Acids Res. 28*, 235–242.
47. Case, D. A., Pearlman, D. A., Caldwell, J. W., Cheatham, T. E. I., Wang, J., Ross, W. S., Simmerling, C. L., Darden, T. A., Merz, K. M., Stanton, R. V., Cheng, A. L., Vincent, J. J., Crowley, M., Tsui, V., Gohlke, H., Radmer, R. J., Duan, Y., Pitera, J., Massova, I., Seibel, G. L., Singh, U. C., Weiner, P. K., and Kollman, P. A. (2002) *AMBER 7*, University of California, San Francisco, CA.
48. Xie, X. M., Geacintov, N. E., and Broyde, S. (1999) Stereochemical origin of opposite orientations in DNA adducts derived from enantiomeric *anti*-benzo[*a*]pyrene diol epoxides with different tumorigenic potentials. *Biochemistry 38*, 2956–2968.
49. Perlow, R. A., and Broyde, S. (2002) Toward understanding the mutagenicity of an environmental carcinogen: Structural insights into nucleotide incorporation preferences. *J. Mol. Biol. 322*, 291–309.
50. Delano, W. L. (2002) *The PyMOL Molecular Graphics System*, DeLano Scientific, San Carlos, CA.
51. Batra, V. K., Beard, W. A., Shock, D. D., Krahn, J. M., Pedersen, L. C., and Wilson, S. H. (2006) Magnesium-induced assembly of a complete DNA polymerase catalytic complex. *Structure 14*, 757–766.
52. Ohashi, E., Ogi, T., Kusumoto, R., Iwai, S., Masutani, C., Hanaoka, F., and Ohmori, H. (2000) Error-prone bypass of certain DNA lesions by the human DNA polymerase κ. *Genes Dev. 14*, 1589–1594.
53. Lone, S., Townson, S. A., Uljon, S. N., Johnson, R. E., Brahma, A., Nair, D. T., Prakash, S., Prakash, L., and Aggarwal, A. K. (2007) Human DNA polymerase κ encircles DNA: Implications for mismatch extension and lesion bypass. *Mol. Cell 25*, 601–614.
54. Seo, K.-Y., Nagalingam, A., Shadi Miri, J. Y., Kolbanovskiy, A., Shastry, A., and Loechler, E. L. (2006) Mirror image stereoisomers of the major benzo[*a*]pyrene N2-dG adduct are bypassed by different lesion-bypass polymerases in *E. coli. DNA Repair 5*, 515–522.

BI701839Q